Stability of Networking DC Microgrids with Active Loads

Marco Carnaghi, Marcos Judewicz, Paula Cervellini, Rogelio Garcia Retegui, and Marcos A. Funes

***Abstract*—Direct current networking microgrids (NMGs) have gained prominence as a means to integrate renewable energy sources and enhance system resilience and robustness through the interconnection of nearby microgrids, typically using cooperative and distributed control strategies. However, they offer a complex scenario regarding stability as they are strongly influenced by several aspects such as delays in the communication network, fluctuating renewable energy sources and presence of multiple uncertain loads spread across the different buses. Despite the aforementioned challenges having been addressed in the literature, a comprehensive simultaneous analysis and coverage of all aspects is yet to be undertaken. With the aim to fill a gap in the knowledge, in this paper, a delay-dependent stability analysis for NMGs is presented, with a specific focus on robust operation in the presence of active loads. The formulation also accounts for the uncertain and varying nature of loads within microgrids. The purpose of the study is to assess the extent to which active loads and communication delays impose more stringent constraints on feasible operating conditions, consensus matrix design, and controller tuning. Circuit simulations are carried out to compare and ratify the insights derived from the stability analysis predicted by the study.**

Link to graphical and video abstracts, and to code: https://latamt.ieeer9.org/index.php/transactions/article/view/8971

***Index Terms*—Networking DC microgrid, Robust Stability, Distributed consensual control, Constant power load, Time-delay**

ACRONYMS

CLT	Closed Loop Transfer function.
CPL	Constant Power Load.
CPS	Constant Power Source.
DER	Distributed Energy Resources.
DG	Distributed Generator.
LMI	Linear Matrix Inequality.
MPPT	Maximum Power Point Tracking.
NMG	Networking Microgrid.
PCC	Point of Common Coupling.
RES	Renewable Energy Sources.

The associate editor coordinating the review of this manuscript and approving it for publication was José Miguel Sosa (*Corresponding author: Marco Carnaghi*).

This work was supported in part by the Universidad Nacional de Mar del Plata (UNMDP), the Consejo Nacional de Investigaciones Científicas y Tecnológicas (CONICET), Argentina.

M. Carnaghi, M. Judewicz, P. Cervellini, R. G. Retegui, and M. A. Funes are with ICyTE - UNMDP - CONICET, Mar del Plata, Buenos Aires, Argentina (e-mails: mcarnaghi@fi.mdp.edu.ar, marcosj@fi.mdp.edu.ar, paulacervellini@fi.mdp.edu.ar, rgarcia@fi.mdp.edu.ar, and mfunes@fi.mdp.edu.ar).

I. INTRODUCTION

DC microgrids are considered efficient due to their use of DC technology and are gaining popularity for integrating distributed energy resources (DERs) [1]. Networking microgrids (NMGs) take this a step further by enhancing DER integration and system robustness through the interconnection of nearby microgrids, typically utilizing cooperative and distributed control strategies. NMGs aim to optimize resource utilization, enhance grid stability, and promote energy system sustainability [2]. However, ensuring the stability of NMGs presents significant challenges due to two main factors: the negative impedance behavior of active loads and time delays in the digital communications of distributed control.

Active loads in NMGs often act as constant power loads (CPLs), introducing nonlinear characteristics and negative impedance [3]. Distributed control strategies rely on communication networks to exchange data among leader controllers. However, the inherent time delays in communication between neighboring participants can significantly affect the stability of NMG systems [2]. These challenges are further accentuated by uncertainties in system loads and the intermittent nature of renewable energy sources (RES) generation [3]–[6].

Several studies have addressed stability in microgrids, considering factors such as uncertain CPLs, RES generation, and communication time-delays. Most studies have focused on stability considering either CPLs or communication delays individually, with only a few attempting to address both simultaneously. For instance, in [3], [7], [8], the stability analysis considering multiple and uncertain active loads is addressed, but the analysis of the impact of time-delays remains pending. Although [3], [7] are not focused on NMG scenarios, the multi-bus representation considered allows for modeling an NMG system. Nevertheless, [3], [7] consider decentralized control strategies (droop control and virtual impedance) aimed at autonomous operation, thus not focusing on cooperative operation of the distributed generation (DG). As a result, the entire NMG acts as a group of stable but independent generators. In [9]–[11], time-delay models for single and multi-bus microgrids are proposed to study delay-dependent stability, but they focus on scenarios with passive loads. Although, all three studies consider distributed control strategies suitable for NMGs, the passive load assumption leads to a linear relationship between the DG's output currents and output voltages, which is not applicable

TABLE I
COMPARISON OF SURVEYS ON THE STABILITY OF DC MICROGRID AND NMGS

Reference	Type of Loads	Loads Uncertainties	Control Scheme	Delay	Microgrid Topology
[3]	CPLs	Considered - Polytopic Sets	Standard Droop Control	Not Considered	MultiBus - NMG compatible
[7]	CPLs	Considered - Bounded Sets	Virtual Resistance and Virtual Inductance	Not Considered	MultiBus - NMG compatible
[8]	CPLs	Considered - Polytopic Sets	Distributed Adaptive Droop Control	Not Considered	MultiBus - NMG compatible
[9]	Resistive	Not Considered	Distributed Consensus-based Control	Fixed and Varying Time delays	Single Bus
[10]	Resistive and CCL	Not Considered	Multiple Distributed Droop-based Control	Fixed Time delays	MultiBus - NMG compatible
[11]	Resistive	Not Considered	Multilayer Distributed Consensus-based Control	Varying Time delays	MultiBus - NMG compatible
[12]	CPL	Not Considered	Distributed Consensus-based Control	Varying Time delays	Single Bus
[13]	CPL	Not Considered	Distributed Consensus-based Control	Varying Time delays	Single Bus

in scenarios with active loads. In an attempt to bridge this gap, [12] and [13] have explored the stability of a single-bus DC microgrid with distributed control, considering both active and passive loads, as well as communication time delays among local controllers. These studies introduced how active loads affect DC microgrid stability in the presence of time delays, but the analysis is not directly extendable to microgrids with multiple buses, loads, and RESs spread across those buses. Moreover, in [9]–[13], uncertainties in loads and RES generation are not incorporated into the stability evaluations performed.

To compare the scope of the works related to the stability analysis of microgrids, Table I summarizes the list of references with the parameters considered relevant in the operation of an NMG. In this context, the type of load considered, the inclusion of uncertainties in the loads, the control strategy utilized, the incorporation of delays in communications, and the topological representation used are considered. When focusing on works that are compatible with the study of NMGs [3], [7], [8], [10], [11], it can be seen that, although these works have provided valuable information, they do not cover all the necessary aspects for the comprehensive evaluation of NMGs. Therefore, it is necessary to address the interplay of multiple uncertain loads (both passive and active) spread across the buses of the NMG, fluctuating RESs, and communication delays inherent to real-world NMG systems.

This paper aims to fill the gap in the existing literature concerning microgrid stability. It focuses on evaluating the stability of NMGs under conditions that have not been comprehensively explored in previous studies yet. Specifically, this study delves into the effects of multiple loads distributed across NMG buses, the influence of different load types, and the implications of controller and consensus gain tuning on NMG stability and performance. To achieve this goal, a state-space model is employed to represent the time-delayed system of an NMG with multiple Points of Common Couplings (PCCs), using a distributed consensual control strategy that has been previously validated in academic literature. Stability conditions are formulated using a delay-dependent Lyapunov approach, which addresses uncertainties in loads and RESs generation through the theory of convex polytopic sets. These sets are defined based on the minimum and maximum values of the variables in the case study. Subsequently, circuit simulations are carried out to compare and validate the insights derived from the stability analysis proposed in this study. The simulation environment includes detailed models of DGs, incorporating local controller tuning, multiple active and passive loads at each bus, and additional communication time delays for local distributed controllers.

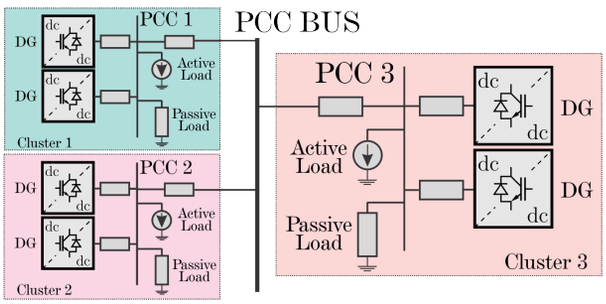

Fig. 1. Representation of an NMG with a multi-cluster approach.

II. MODELING THE NMG

Modeling an NMG involves representing the multi-bus microgrid configuration, formulating equations to characterize the circuit, capturing the control dynamics of the local models, and incorporating time delays into the derived expressions [3], [14]. To simplify the modeling process and focus on the essential dynamics, a model-order reduction approach is employed. This apporach involves neglecting the high-frequency dynamics within each DC microgrid to concentrate on the low-frequency dynamics of the NMG-level control scheme [13], [15], [16]. Aligned with such approach, the term "cluster" will be used to denote each microgrid of the NMG operating with a distributed control strategy for cooperative action [2], [11]. All considerations made are described in the following sections.

A. Multi-cluster NMG Representation

The NMG depicted in Fig. 1 comprises interconnected clusters that group distributed generators and loads in close proximity to each other. A representation of each cluster

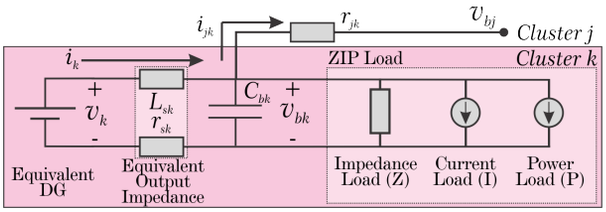

Fig. 2. Representation of an equivalent cluster.

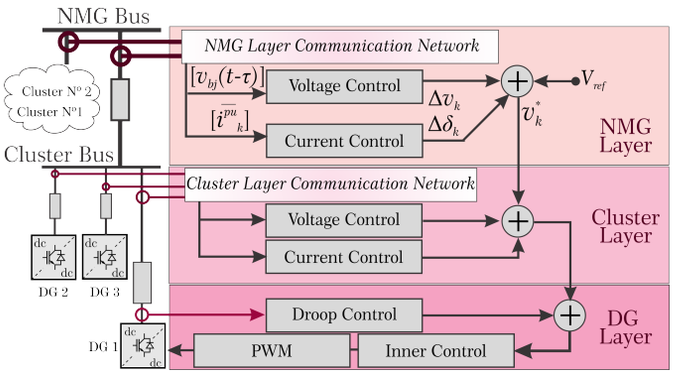

Fig. 3. Hierarchical control scheme.

is shown in Fig. 2, where DGs, loads, and connection impedances are grouped and replaced by equivalent models. Various considerations are made regarding the elements within each individual cluster. The control strategy associated with each power converter operating in voltage mode adopts a common scheme, as shown in Fig. 3 [2], [11]. The control scheme is organized in a cascaded multilayer configuration. The DG layer determines control actions based on local measurements, the cluster layer derives control actions through information exchange among DGs and variables measured within a cluster, and the NMG layer orchestrates control actions based on information exchange among various clusters in a distributed manner.

The analysis focuses on the NMG's distributed control layer, responsible for establishing a common voltage reference input (v_k^*), shared among all local controllers within a given cluster [11]. To reduce system complexity and study network-level dynamics, a proper dynamic separation is maintained between different layers of the control hierarchy. The controllers associated with the NMG layer operate with significantly lower bandwidth compared to those in the cluster and DG layers [15], [16]. In Fig. 2, the controllable voltage source (v_k) is defined for the NMG layer to capture its behavior, which is shared across all DGs within a cluster. The aggregated output current of the DGs within each cluster is denoted as i_k, which corresponds to the output current of the voltage source v_k. For interconnections between the outputs of DGs and the local DC bus, equivalent connection impedances (L_{sk} and r_{sk}) and DC-link capacitance (C_{bk}) are defined assuming close proximity of the different PCCs within a given cluster [13]. A ZIP load model is used to represent the load in each cluster [16], [17]. Resistive interconnection impedances (r_{jk}) are considered to interconnect the DC buses of the clusters. These interconnections are established based on the NMG's topology, using principles of graph theory and employing an undirected graph model [2], [9].

B. Dynamic Model of the kth-cluster

The model of each individual cluster can be derived from the expressions of the control strategy and the equivalent output circuit, which includes L_{sk}, r_{sk}, C_{bk}, and the ZIP load. The original ZIP load model represents load behavior as a combination of constant impedance (Z), constant current (I), and constant power (P) components in relation to bus voltage. While effective for certain applications, this static model is insufficient for capturing the characteristics of microgrid loads, which exhibit significant variations. To address this limitation, the present article adopts a two-tiered approach.

Firstly, a linearized ZIP model is employed to analyze small-signal stability around an equilibrium point [3], [16]. Secondly, in the following section, the representation is extended to account for load uncertainties that do not correspond to small-signal changes, but rather to large-signal variations that alter the system response [3], [8].

1) Control loop model: The analysis primarily focuses on the NMG distributed control layer shown in Fig. 3, which aims to track the NMG's reference voltage and achieve current sharing among clusters. A representation of the control layer is depicted in Fig. 4 and is used to derive expressions that describe its behavior.

The voltage reference v_k^* is calculated as follows:

$$v_k^* = V_{ref} + \Delta v_k - \Delta\delta_k \tag{1}$$

Here, V_{ref} is the DC bus voltage reference. Δv_k is the output of the voltage I_v controller, with parameter k_{VI_k}, used to ensure that the average DC bus voltage $v_{NMG} = \frac{1}{n}\sum_{j=1}^{N} v_{bk}$ converges to its reference value V_{ref}:

$$\Delta v_k = k_{VIk}\int (V_{ref} - v_{NMG})dt \tag{2}$$

Additionally, $\Delta\delta_k(t)$ is the output of the current PI_i controller used for load sharing among the clusters. The operation of this distributed current controller relies on information exchange among the clusters and local data measurements. To ensure that every node can communicate with every other node, directly or indirectly, a sparse communication network must be designed to satisfy the global reachability condition [9]. The following consensus expression is used to adjust the current reference i_k^* of the k-th cluster based on the current references i_j^* of the j-th cluster:

$$\dot{i_k^*} = -\sum_{j=1, j\neq k}^{N} a_{kj}(i_k^* - i_j^*) \tag{3}$$

Here, a_{kj} are the coefficients that describe the communication links among the clusters and define the weights of the interchanged information among them. If there is a communication link from the k-th to the j-th cluster, then $a_{kj} > 0$; otherwise, $a_{kj} = 0$ [3], [9]. The adjacency matrix

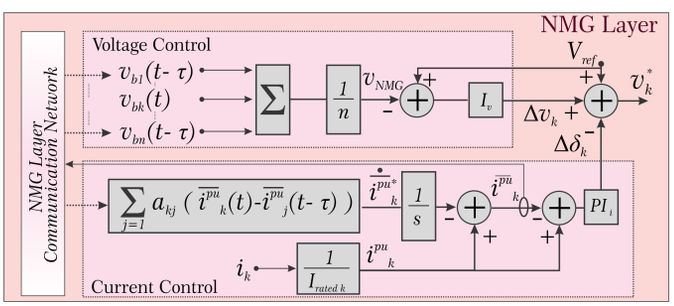

Fig. 4. Distributed control framework for the NMG model.

$A_G = [a_{ij}] \in \Re^{(nxn)}$ determines the changes of the n current references. The expression above can be rewritten in matrix form using the Laplacian matrix L:

$$\dot{I^*} = -LI^* \tag{4}$$

Here, $I^* = [i_1^*, i_2^*, ..., i_n^*]$, and:

$$L = D_G^{in} - A_G \tag{5}$$

where D_G^{in} is the indegree matrix associated with A_G, a diagonal matrix whose elements are defined by $\sum_{j \in N_k} a_{kj}$. The eigenvalues of L determine the dynamics of I^*, so the coefficients a_{kj} must be defined to ensure stable behavior. At steady state, $\dot{I} \to 0$ and $i_k^* \approx i_j^*$ for $k, j = 1, 2, ..., n$.

To achieve current sharing proportional to the equivalent nominal current of each cluster, a change of variables is employed:

$$\overline{i_k^{pu}} = i_k^* / I_{rate_k} \ , \ \ i_k^{pu} = i_k / I_{rate_k} \tag{6}$$

Here, while i_k is the current injected into the local bus of the k-th cluster, I_{rate_k} is the equivalent nominal current of the k-th cluster. The reference for the current-sharing PI controller, as shown in Fig. 4, is:

$$\overline{i_k^{pu}}(t) = i_k^{pu}(t) - \int \sum_{j=1}^{N} a_{kj} (\overline{i_k^{pu}}(t) - \overline{i_j^{pu}}(t)) dt \tag{7}$$

The sum over all clusters j accounts for the contribution of each cluster to the total current reference for the k-th cluster. The correction term $\Delta\delta_k(t)$ for the current controller is then calculated as:

$$\Delta\delta_k(t) = k_{CPk}(i_k^{pu}(t) - \overline{i_k^{pu}}(t)) + k_{CIk} \int (i_k^{pu}(t) - \overline{i_k^{pu}}(t)) dt \tag{8}$$

Here, k_{CP_k} and k_{CI_k} are the proportional and integral coefficients of the PI controller, respectively.

To account for the varying time delays (τ) in the information exchange within the distributed control layer, the expressions are modified as follows:

$$\Delta v_k(t) = k_{VIk} \int (V_{ref} - v_{NMG}(t - \tau)) dt \tag{9}$$

$$\overline{i_k^{pu}}(t) = i_k^{pu}(t) - \int \sum_{j=1}^{N} a_{kj} (\overline{i_k^{pu}}(t) - \overline{i_j^{pu}}(t - \tau)) dt \tag{10}$$

The transmission time delay primarily affects variables originating from the NMG layer communication network, as illustrated. Conversely, other variables considered in the expressions are derived from local measurements within each specific cluster. The findings presented in [18] suggest that local measurements should have shorter delays and faster controllers compared to those in the NMG layer. This differentiation helps prevent the system from being overly constrained by time delay conditions.

2) Output circuit model: The cluster model, represented in Fig. 2, is described by the following equations:

$$\begin{aligned} \dot{i_k} &= \frac{1}{L_{sk}} [v_k - v_{bk} - r_{sk} i_k] \\ &= \frac{1}{L_{sk}} [V_{ref} + \Delta v_k - \Delta\delta_k - v_{bk} - (r_{sk}) i_k] \end{aligned} \tag{11}$$

$$\dot{v_{bk}} = \frac{1}{C_{bk}} [i_k - \sum_{j=1, j \neq k} g_{kj} (v_{bk} - v_{bj})$$

$$\frac{p_{cpl_k}}{v_{bk}} \approx \frac{P_{cpl_k}^{eq}}{V_{bk}^{eq}} + \frac{P_{cpl_k}^{eq}}{-(V_{bk}^{eq})^2} v_{ck} \approx I_{cplk} + g_{cpl_k} v_{bk} \tag{12}$$

$$i_{load_k} - \frac{p_{cpl_k}}{v_{bk}}] \tag{13}$$

where:

- $g_{kj} = g_{jk} = r_{jk}^{-1} \in \Re^+$ is the conductance of the distribution line between the k-th and j-th buses.
- $g_{load_k} \in \Re^+$ is the conductance of the impedance load (Z) in the k-th bus.
- $i_{load_k} \in \Re$ is the current associated with the current load (I) in the k-th bus.
- $I_{cpl_k} \in \Re$ is the constant current source defining the linearization point for the k-th CPL in equation (13).
- $g_{cpl_k} \in \Re$ is the incremental conductance associated with the k-th CPL.
- $v_k \approx v_k^*$ due to considerations made regarding control dynamics.

The terms i_{load_k}, I_{cpl_k}, and g_{cpl_k} are expressed in $\Re$ to allow for modeling RESs operating in Maximum Power Point Tracking (MPPT) mode, functioning as constant power sources (CPS), or CPLs with inverted power or current flow [13].

3) Overall model: The global model of the NMG system is expressed as follows:

$$\dot{\mathbf{X}} = \mathbf{A}.\mathbf{X} + \mathbf{B}.\mathbf{X}_\tau + \mathbf{H_1} V_{ref} + \mathbf{H_2} \mathbf{I_{tot}} \tag{14}$$

Where:

$$\begin{aligned} \mathbf{X} &= [\mathbf{V_b}, \mathbf{\Delta}, \mathbf{I}, \mathbf{I^{pu}}]^T \in \Re^{4n} \\ \mathbf{X}_\tau &= [\mathbf{V_b}(\mathbf{t} - \tau), \mathbf{\Delta}(\mathbf{t} - \tau), \mathbf{I}(\mathbf{t} - \tau), \mathbf{I^{pu}}(\mathbf{t} - \tau)]^T \in \Re^{4n} \\ \mathbf{V_b} &= [v_{b1}, ..., v_{bn}]^T \in \Re^n \\ \mathbf{I} &= [i_1, ..., i_n]^T \in \Re^n \\ \mathbf{I^{pu}} &= [\overline{i_1^{pu}}, ..., \overline{i_n^{pu}}]^T \in \Re^n \\ \mathbf{\Delta} &= [\Delta v_1 - \Delta\delta_1, ..., \Delta v_n - \Delta\delta_n]^T \in \Re^n \\ \mathbf{I_{tot}} &= [I_{cpl_1} + i_{load_1}, ..., I_{cpl_n} + i_{load_n}]^T \in \Re^n \end{aligned}$$

The matrices $\mathbf{A}$, $\mathbf{B}$, $\mathbf{H_1}$, and $\mathbf{H_2}$ result from the matrix representation of the coefficients shown in equations (8)-(13), with their final expressions provided in the appendix.

In the term associated with $\mathbf{I_{tot}}$ in equation (14), it is shown that changes in the values of i_{load_k} do not result in changes in the coefficients of matrices $\mathbf{A}$ and $\mathbf{B}$. Therefore, current loads do not affect the stability of the system, and as such, they are not considered in the stability formulation hereafter.

III. Robust Stability Analysis

Once the global model of the NMG system is defined as in equation (14), the next step is to evaluate the system's stability. In this article, a time-domain analysis method is employed for this purpose, with the aim of formulating stability conditions

as a Linear Matrix Inequality (LMI) problem [3], [9]. Initially, the problem is defined for a single operating point and is then expanded to consider multiple operating conditions using convex polytopic theory to model uncertain parameters.

A. Nominal System

The system with a time-varying delay is represented, as follows [9], [19]:

$$\dot{\mathbf{X}}(t) = \mathbf{A}.\mathbf{X}(t) + \mathbf{B}.\mathbf{X}(t-\tau(t)), \;\; t > 0 \tag{15}$$

$$\mathbf{X}(t) = \mathbf{\Phi}(t), \;\; t \in [-\tau^*, 0] \tag{16}$$

Here, $\tau(t)$ is a time-varying, differentiable function that satisfies:

$$0 \leq \tau(t) \leq \tau^* \;,\; |\dot{\tau(t)}| \leq \mu \tag{17}$$

where μ and τ^* are constant upper bounds, and $\mathbf{\Phi}(t)$ is the initial condition vector function.

For the system (15), the following theorem states a stability condition in the form of an LMI problem. The proof of the theorem can be found in [19].

Theorem 1: Given scalars $\tau^* > 0$ and μ, the system (15) with a time-varying delay $\tau(t)$ satisfying (17) is asymptotically stable if there exist matrices $\mathbf{P} = \mathbf{P}^T > 0$, $\mathbf{Q} = \mathbf{Q}^T > 0$, $\mathbf{R} = \mathbf{R}^T \geq 0$, $\mathbf{Z}_i = \mathbf{Z}_i^T > 0$ for $i = 1, 2$, and the free weight matrices:

$$\mathbf{N} = \begin{bmatrix} \mathbf{N_1} \\ \vdots \\ \mathbf{N_4} \end{bmatrix} \;\; \mathbf{S} = \begin{bmatrix} \mathbf{S_1} \\ \vdots \\ \mathbf{S_4} \end{bmatrix} \;\; \mathbf{M} = \begin{bmatrix} \mathbf{M_1} \\ \vdots \\ \mathbf{M_4} \end{bmatrix} \;\; \mathbf{T} = \begin{bmatrix} \mathbf{T_1} \\ \vdots \\ \mathbf{T_4} \end{bmatrix} \tag{18}$$

and the following conditions are satisfied:

$$\begin{bmatrix} \mathbf{\Theta} & \tau^*\mathbf{N} & \tau^*\mathbf{S} & \tau^*\mathbf{M} \\ * & -\tau^*\mathbf{Z_1} & 0 & 0 \\ * & * & -\tau^*\mathbf{Z_1} & 0 \\ * & * & * & -\tau^*\mathbf{Z_2} \end{bmatrix} < 0 \tag{19}$$

where

$$\mathbf{\Theta} = \mathbf{\Theta_1} + \mathbf{\Theta_2} + \mathbf{\Theta_2^T} \tag{20}$$

$$\mathbf{\Theta_1} = \begin{bmatrix} \mathbf{Q}+\mathbf{R} & 0 & 0 & \mathbf{P} \\ * & -(1-\mu)\mathbf{Q} & 0 & 0 \\ * & * & -\mathbf{R} & 0 \\ * & * & * & \tau^*(\mathbf{Z_1}+\mathbf{Z_2}) \end{bmatrix} \tag{21}$$

$$\mathbf{\Theta_2} = \begin{bmatrix} \mathbf{N}+\mathbf{M} & -\mathbf{N}+\mathbf{S} & -\mathbf{M}-\mathbf{S} & 0 \end{bmatrix} + \mathbf{T\Lambda} + \mathbf{\Lambda^T T^T} \tag{22}$$

$$\mathbf{\Lambda} = \begin{bmatrix} -\mathbf{A} & -\mathbf{B} & 0 & \mathbf{I} \end{bmatrix} \tag{23}$$

This theorem provides a method to check the stability of a system with time-varying delays by formulating it as an LMI problem. The conditions ensure that the system remains stable even with varying delays within certain bounds. Note that the obtained stability conditions are sufficient but not necessary, since they are derived from the Lyapunov stability criterion from time-varying systems. Additionally and as a consequence of the conditions imposed on the derivative of the Lyapunov functional, the conditions in Theorem 1 ensure asymptotic stability of the System in equation (15) [19].

B. Uncertain System

This section extends the analysis from Theorem 1 to incorporate uncertainties arising from varying loads and renewable generation into the model's stability assessment, particularly focusing on steady-state conditions. The system model (14) is expressed with polytopic-type uncertainties, meaning the system matrices must satisfy the real convex polytopic constraints:

$$[\mathbf{AB}] \in \Omega,$$

$$\Omega = [\mathbf{A}(\epsilon)\mathbf{B}(\epsilon)] = \sum_{j=1}^{p} \epsilon_j [\mathbf{A}_j \mathbf{B}_j], \;\; \sum_{j=1}^{p} \epsilon_j = 1, \epsilon_j \geq 0 \tag{24}$$

where $\mathbf{A}_j$, $\mathbf{B}_j$ for $j = 1, ..., p$, are constant matrices with appropriate dimensions, and ϵ_j for $j = 1, ..., p$, represent the system uncertainties [19].

These uncertainties arise from the changing power demanded by loads and generated by renewable energy sources. The uncertainties related to power demanded by CPLs and CPSs are represented as a bounded polytopic set $\check{P}$ defined as:

$$\check{P} = \{p : p_k \in [\underline{p_k}, \overline{p_k}], k = 1, ..., n\} \tag{25}$$

Here, $\underline{p_k}$ and $\overline{p_k}$ represent the minimum and maximum values of power consumed or generated by the k-th CPL or non-dispatchable power source. The uncertainties that arise from the linearization of power flow (g_{cpl_k} in (13)) also depend on DC bus voltage setpoints for steady-state operation. The DC bus voltage setpoints during steady-state operation are represented as ν_{eq}^b, defined as:

$$\nu_b^{eq} = \{V_b^{eq} \in \mathbb{R}^n : v_{bk}^{eq} \in [\underline{v_{bk}}, \overline{v_{bk}}], k = 1, ..., n\} \tag{26}$$

where $\overline{v_{bk}} > \underline{v_{bk}} > 0$ represent their maximum and minimum bounds. Similarly, uncertainties associated with resistive load components are represented in a polytopic set $\check{G}$:

$$\check{G} = \{g_{load} : g_{load_k} \in [\underline{g_{load_k}}, \overline{g_{load_k}}], k = 1, ..., n\} \tag{27}$$

where $\underline{g_{load_k}}$ and $\overline{g_{load_k}}$ represent the minimum and maximum values of the load conductance associated with the k-th cluster.

Once the vertex cases of $\check{G}$, ν_b^{eq}, and $\check{P}$ are defined, the vertex system matrices $\mathbf{A}_j$ and $\mathbf{B}_j$ in (24) can be calculated. The stability analysis is then extended to account for these polytopic-type uncertainties as follows [19] :

Theorem 2: Given scalars $\tau^* > 0$ and μ, the system (15) with polytopic-type uncertainties satisfying (24) and a time-varying delay $\tau(t)$ satisfying (17) is robustly stable if there exist matrices $\mathbf{P}_j = \mathbf{P}_j^T > 0$, $\mathbf{Q}_j = \mathbf{Q}_j^T > 0$, $\mathbf{R}_j = \mathbf{R}_j^T \geq 0$, $\mathbf{Z}_{ij} = \mathbf{Z}_{ij}^T > 0$ for $i = 1, 2$, and the free weight matrices:

$$\mathbf{N}_j = \begin{bmatrix} \mathbf{N_1}_j \\ \vdots \\ \mathbf{N_4}_j \end{bmatrix} \;\; \mathbf{S}_j = \begin{bmatrix} \mathbf{S_1}_j \\ \vdots \\ \mathbf{S_4}_j \end{bmatrix} \;\; \mathbf{M}_j = \begin{bmatrix} \mathbf{M_1}_j \\ \vdots \\ \mathbf{M_4}_j \end{bmatrix} \;\; \mathbf{T} = \begin{bmatrix} \mathbf{T_1} \\ \vdots \\ \mathbf{T_4} \end{bmatrix} \tag{28}$$

and the following conditions are satisfied for $j = 1, ..., p$:

$$\begin{bmatrix} \mathbf{\Theta}^{(j)} & \tau^*\mathbf{N}_j & \tau^*\mathbf{S}_j & \tau^*\mathbf{M}_j \\ * & -\tau^*\mathbf{Z_1}_j & 0 & 0 \\ * & * & -\tau^*\mathbf{Z_1}_j & 0 \\ * & * & * & -\tau^*\mathbf{Z_2}_j \end{bmatrix} < 0 \tag{29}$$

where

$$\boldsymbol{\Theta}^{(j)} = \boldsymbol{\Theta_1}^{(j)} + \boldsymbol{\Theta_2}^{(j)} + [\boldsymbol{\Theta_2}^{(j)}]^T \tag{30}$$

$$\boldsymbol{\Theta_1}^{(j)} = \begin{bmatrix} \mathbf{Q}_j + \mathbf{R}_j & 0 & 0 & \mathbf{P}_j \\ * & -(1-\mu)\mathbf{Q}_j & 0 & 0 \\ * & * & -\mathbf{R}_j & 0 \\ * & * & * & \tau^*(\mathbf{Z_1}_j + \mathbf{Z_2}_j) \end{bmatrix} \tag{31}$$

$$\boldsymbol{\Theta_2}^{(j)} = \begin{bmatrix} \mathbf{N}_j + \mathbf{M}_j & -\mathbf{N}_j + \mathbf{S}_j & -\mathbf{M}_j - \mathbf{S}_j & 0 \end{bmatrix} + \mathbf{T}\boldsymbol{\Lambda}_j + \boldsymbol{\Lambda}_j^T\mathbf{T}^\mathbf{T} \tag{32}$$

$$\boldsymbol{\Lambda}_j = \begin{bmatrix} -\mathbf{A}_j & -\mathbf{B}_j & 0 & \mathbf{I} \end{bmatrix} \tag{33}$$

The proof of Theorem 2, which extends the stability method to evaluate the delay-dependent stability of the system (14) under time-varying delays, can be found in [19]. This theorem accounts for the uncertain nature of power loads or generation within each cluster, as expressed in (25), (26), and (27).

IV. Stability Evaluation

In this section, a four-cluster NMG is evaluated as a case study. The parameters for the NMG, listed in Table II, were partially derived from the analysis performed in [20]. The evaluation is based on the mathematical model and formulations presented in the previous sections.

The CVX Research library for MATLAB is used to develop the convex formulations and perform four different analyses [9], [21]. The first analysis examines the impact of total load power and its distribution among the clusters. The second analysis focuses on the effects of consensus gains, while the third explores the tuning of controller gains. Lastly, the fourth analysis studies the impact of active and passive load proportions on the stability margin of the NMGs. All analyses cover scenarios involving both, active and passive loads, and consider a delay range from $10\,\mathrm{ms}$ to $800\,\mathrm{ms}$, based on values previously reported [9]–[11]. All the analyses follow the same procedure to determine the maximum communication delay (τ^*_{max}) under given operating conditions. The value of τ^*_{max} is defined when the LMI existence problem in Theorem 2 transitions from feasible to infeasible. Specifically, this occurs when an incremental change in τ^* (evaluated in steps of $10\,\mathrm{ms}$ throughout the current section) results in no set of matrices that can simultaneously satisfy all the conditions outlined in Theorem 2. Consequently, it can no longer be verified that the system meets the sufficient stability conditions using the proposed Lyapunov functional. This transition defines the maximum communication delay for which the formulation can guarantee stability under the specified operating conditions.

A. Power Distribution Impact on NMG Stability

Simulations were conducted to analyze the impact of total load power (P_{tot}), its distribution among clusters, and the type of load on The parameter P_{tot} represents the total power that the DGs in voltage mode must provide. It is calculated as the difference between the load power and the power contributed by CPSs. Specifically, the goal is to analyze how τ^*_{max} changes with an increasing upper bound of the total load power $\overline{P_{tot}}$ in the NMG and how it is affected by different power distribution scenarios. $\overline{P_{tot}}$ is defined as:

$$\overline{P_{tot}} = \sum_{j=0}^{n} \overline{p_j} \tag{34}$$

where $\overline{p_j}$ is the upper bound of the load power in the j-th cluster.

To achieve this goal, an iterative process is followed where $\overline{P_{tot}}$ is increased, and the $\overline{p_k}$ values are calculated based on different power distribution scenarios listed in Table III to define the vertex system matrices for the formulation. For each scenario, an LMI problem is formulated and solved iteratively, increasing τ^* to determine the values of τ^*_{max}.

The simulations are conducted across three distinct power distribution scenarios. These scenarios manipulate the fraction of P_{tot} connected to each cluster, thereby studying power flow interactions and their effects on the overall system stability. Two different load types are considered: purely CPLs, using the formulation presented in (25), and purely resistive loads, using the formulation presented in (27).

1) Active loads case (purely CPLs): The solid line curves in Fig. 5 illustrate the relationship between τ^*_{max} and $\overline{P_{tot}}$ for each power distribution scenario in Table III, specifically considering the results obtained for CPLs. The curves depict the critical points at which stability is guaranteed for the given τ^* and total power load upper value. Operating below these curves ensures stability, as the LMI formulation provides sufficient conditions. Operating above the curves introduces uncertainty, as stability cannot be assured. The system might still remain stable, but this cannot be guaranteed.

The uncertainty in the variation of each p_k is accounted for using the vertex cases of the polytopic formulation. For example, consider the point [$\overline{P_{tot}} = 200\,\mathrm{kW}$, $\tau^*_{max} = 500\,\mathrm{ms}$] within the curve associated with Distribution No. 1. This point indicates that the system remains stable for any combination of $\{\ p_1 = [6\,\mathrm{kW}, 20\,\mathrm{kW}]$, $p_2 = [18\,\mathrm{kW}, 60\,\mathrm{kW}]$, $p_3 = [27\,\mathrm{kW}, 90\,\mathrm{kW}]$, $p_4 = [9\,\mathrm{kW}, 30\,\mathrm{kW}]\ \}$ as long as $\tau^* \leq \tau^*_{max} = 500\,\mathrm{ms}$.

The curves for scenarios with active loads demonstrate that a balanced power distribution shifts the overall curve, allowing it to accommodate longer delays while maintaining the same $\overline{P_{tot}}$. A more balanced distribution implies that clusters with larger loads also have a greater influence in the power-sharing control, as reflected in the I_{rate_k} values in Table II. The second

TABLE II
Parameters for 4-Cluster NMG

Param.	Value	Param.	Value	Param.	Value
r_{s_1}	0.25Ω	L_1	$0.75\,\mathrm{mH}$	C_{b_1}	$1.70\,\mathrm{mF}$
r_{s_2}	0.53Ω	L_{s_2}	$0.90\,\mathrm{mH}$	C_{b_2}	$1.00\,\mathrm{mF}$
r_{s_3}	0.20Ω	L_{s_3}	$1.25\,\mathrm{mH}$	C_{b_3}	$0.80\,\mathrm{mF}$
r_{s_4}	0.50Ω	L_{s_4}	$0.80\,\mathrm{mH}$	C_{b_4}	$1.10\,\mathrm{mF}$
g_{12}	$1.20\Omega^{-1}$	g_{13}	$0.30\Omega^{-1}$	g_{14}	$0.00\Omega^{-1}$
g_{23}	$0.00\Omega^{-1}$	g_{24}	$1.55\Omega^{-1}$	g_{34}	$0.75\Omega^{-1}$
k_{VI_k}	1.00	k_{CI_k}	10.0	k_{CP_k}	0.50
$\overline{V_{ref}}$	1050 V	$\underline{V_{ref}}$	950 V	$I_{rate\ 1}$	100 A
$I_{rate\ 2}$	50 A	$\overline{I_{rate\ 3}}$	33 A	$I_{rate\ 4}$	33 A

TABLE III
POWER DISTRIBUTION SCENARIOS

Distribution Number	Cluster List Nº1	Nº2	Nº3	Nº4
1	10%	30%	45%	15%
2	45%	30%	10%	15%
3	30%	45%	15%	10%

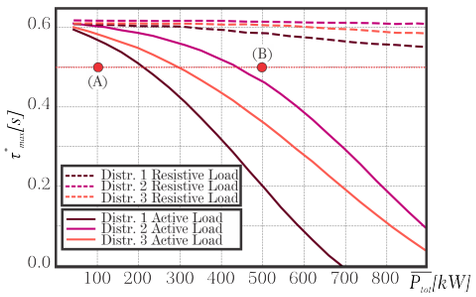

Fig. 5. τ^*_{max} vs. $\overline{P_{tot}}$ for three power distribution scenarios. Solid lines: CPLs; dotted lines: resistive loads. Being A and B operating conditions to be simulated.

case represents a more balanced scenario, where clusters with higher I_{rate} values also contribute a larger percentage of the total load. These findings suggest that the distribution of power among clusters significantly affects the system's ability to tolerate communication delays. A balanced power distribution enables the system to handle longer delays while maintaining stability. The weight of each cluster in the power-sharing control is influenced by its load, which impacts the overall system stability.

2) Comparison with resistive loads case: From the curves shown in Fig. 5, it is observed that under low load conditions, both scenarios –active loads and resistive loads– converge to a common case, establishing an upper limit for τ^*_{max} that the system can withstand regardless of P_{tot}. However, in the scenario with active loads, a significant deterioration of τ^*_{max} becomes evident, highlighting the importance of considering the proportion of active and passive loads within each cluster.

The presence of active loads imposes more stringent constraints on the feasible operating conditions compared to scenarios with only resistive loads. Active loads exhibit negative impedance behavior, which deteriorates the system's damping. The sensitivity of τ_{max} to changes in the distribution of P_{tot} is significantly higher when active loads are involved. The observed deterioration in system damping affects the eigenvalues, with different load distributions leading to changes in the eigenvalues associated with each cluster.

The analysis suggests that the power demanded by active loads and its distribution across the NMGs have a more pronounced impact on the system's stability margin compared to resistive loads.

B. Impact of Consensus Matrix on NMG Stability

This section discusses the analysis of how the consensus matrix coefficients (a_{kj}) influence τ^*_{max} in a distributed and consensual scenario. The variations in τ^*_{max} with respect to P_{tot} are examined for two types of loads: purely resistive loads (Fig. 6(b)) and purely CPLs (Fig. 6 (c)), under identical controller gains and power distribution configurations. The results are obtained for a consensus matrix where $a_{ij} = a$ for $j = i - 1$ and $j = i + 1$, and $a_{ij} = 0$ otherwise. Changes in this matrix (varying parameter a) lead to variations in the system's response. τ^*_{max} is plotted as a function of a and $\overline{P_{tot}}$.

In Fig. 6(a), the Zero-Pole map of the system's Closed Loop Transfer function (CLT) for the purely resistive load scenario is presented. This map provides insights into system stability for different values of a along the trajectory highlighted in Fig. 6(b). As can be seen, both the CLT and the surface indicate that the system reaches a borderline stability condition at approximately $a = 5$. Observing Fig. 6(b) and Fig. 6(c), in both load scenarios, an initial abrupt reduction in τ^*_{max} occurs for small values of a, followed by a smoother trend. For scenarios involving CPLs, this behavior is more pronounced under low load conditions, with τ^*_{max} degrading significantly as $\overline{P_{tot}}$ increases. Increasing a corresponds to a greater gain of the integral controller and increased bandwidth, making the impact of the delay more noticeable under the same operating conditions.

The analysis underscores the importance of carefully designing the consensus matrix to achieve stable and robust operation of the NMG system. Slower consensus (lower a values) enhances robustness against time delays, while aiming for faster consensus (higher a values) leads to a drop in τ^*_{max}. The visual representation of the feasible values for a according to the load, communication matrix, and time delays within the NMG aids in system design and analysis. The intersection of the surface with the plane $a = 1$ is highlighted in Fig. 6(b) and Fig. 6(c), and this intersection corresponds to the curves shown in Fig. 5 for Distribution No. 1, aiding in correlating and interpreting the results.

C. Impact of Integral (I) and Proportional-Integral (PI) controller tuning on NMGs

The goal is to elucidate how controller gains impact the value of τ^*_{max}. The results depicted in Fig. 7 show variations in τ^*_{max} for different values of distributed control gains, considering both CPLs and resistive loads. The graphical representations provide insights into how the system's stability changes with varying controller gains. The methodology outlined below is followed:

- Step 1: define a constant power distribution among the clusters with a fixed value selected for $\overline{P_{tot}}$. Initial values for the controller gains and parameters are determined by analyzing the small-signal block diagram corresponding to the local model of individual clusters.
- Step 2: to create the 3D representations shown in the figures, k_{iv} remains constant while k_{ii} and k_{pi} are varied. For each combination of (k_{iv}, k_{ii}, k_{pi}), the LMI problem is iteratively solved increasing τ^* to determine the values of τ^*_{max}.

Certain combinations of k_{ii} and k_{pi} are excluded from Fig. 7 based on the small-signal analysis. These excluded combinations lead to non-convergent controllers, even without time delays. If the operating conditions of the NMG fall

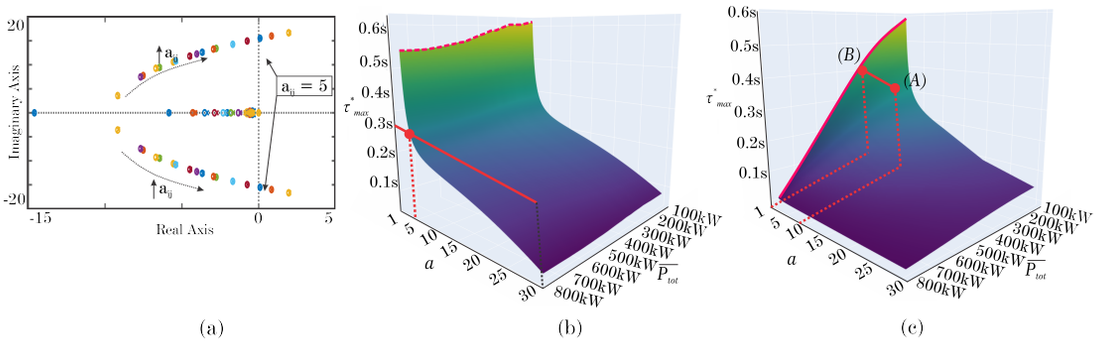

Fig. 6. (a) Zero-Pole Map of the system's Closed-Loop Transfer Function, considering the highlighted red trajectory in (b); (b) τ^*_{max} plotted as a function of $\overline{P_{tot}}$ and the consensus matrix coefficients a for resistive loads. (c) τ^*_{max} plotted as a function of $\overline{P_{tot}}$ and the consensus matrix coefficients a for purely CPLs.

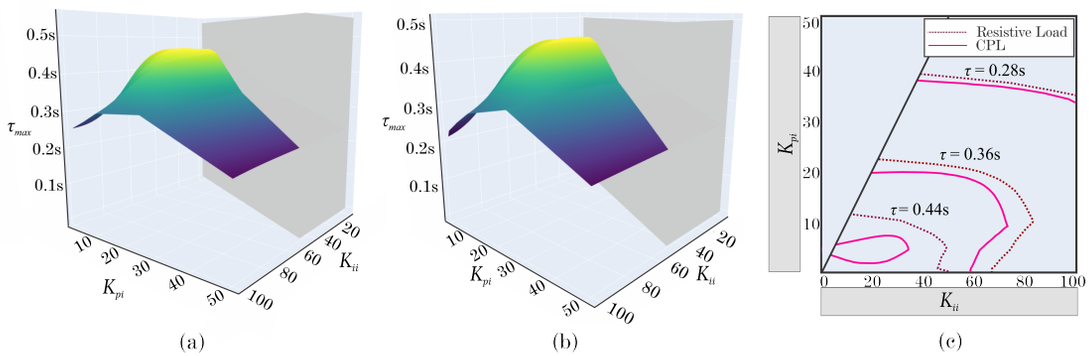

Fig. 7. τ^*_{max} plotted as a function of k_{ii} and k_{pi} for: (a) CPLs and (b) resistive loads. Additionally, (c) shows the contour plot obtained by intersecting the surfaces with constant τ^*_{max} hyperplane conditions. The power distribution scenario No. 1 with $\overline{P_{tot}} = 400\,\text{kW}$ and a constant value of $k_{iv} = 3$ was used to obtain the surfaces.

below the bell-shaped surfaces, system stability is assured. Conditions extending beyond these surfaces in Fig. 7 indicate undefined system stability according to the current method.

The surfaces in Fig. 7 are intersected with three constant τ hyperplane conditions. The contour plot in Fig. 7(c), which shows how these intersections project onto the (k_{ii}, k_{pi}) plane, provides insights into the feasible combinations of controller gains for different τ^* conditions. When considering CPLs, they lead to a more constrained set of feasible combinations of (k_{ii}, k_{pi}) for each τ^* condition. The difference between CPLs and resistive loads diminishes as the value of the τ^* condition decreases. CPLs generally reduce τ^*_{max} for the NMG across the considered combinations of (k_{ii}, k_{pi}). These observations emphasize the critical roles played by controller tuning and the type of loads (CPL or resistive) in achieving stable operation within the NMG system, especially in scenarios involving time delays in the communication network.

D. Impact of Active and Passive loads proportions on NMGs

In previous analyses, only the extreme cases of load types, purely CPLs and purely resistive loads, were considered. This section aims to analyze the system's behavior in intermediate cases between these extremes. Figure 8 shows the variations in τ^*_{max} with respect to α, where α represents the fraction of P_{tot} associated with resistive loads. It is important to note that several parameters of the NMG must remain constant to obtain the curve in Fig. 8. For instance, $\underline{P_{tot}}$, $\overline{P_{tot}}$ and their distribution among the clusters remain constant and follow the load type balance described by α. Specifically, the values $\underline{P_{tot}} = 60\,\text{kW}$ and $\overline{P_{tot}} = 400\,\text{kW}$ were considered. Additionally, the controller gains are kept constant, using the values presented in Table II. The curves in Fig. 8 show a smooth transition from the purely CPLs condition to the purely resistive loads condition shown in Fig. 5, under a constant load boundary condition. It is worth noting the slight bump in τ^*_{max} for conditions close to $\alpha = 0.5$, where the equivalent impedance resulting from the negative impedance of CPLs and the positive value of resistive loads is close to zero. In this scenario, the loads appear as current loads from the perspective of the bus, which do not significantly impact system stability as previously discussed. Therefore, the eigenvalues of the system tend to approach those of the zero load condition, depending on the NMG´s base design. As the system moves away from this condition, τ^*_{max} deteriorates at different rates depending on the predominant type of load.

V. Circuit Simulation

To validate the results obtained from the mathematical model and the presented analysis, the four-cluster NMG is also recreated in a circuit simulation environment developed in MATLAB/Simulink. The main objective of this section is to confirm the findings from the previous section. While simulations cannot capture all scenarios explored in Section

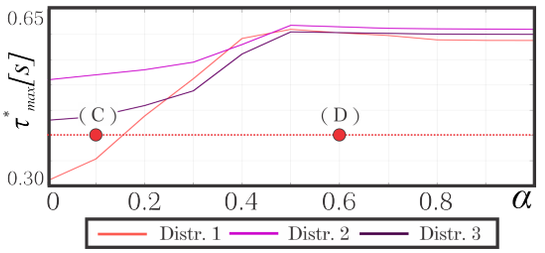

Fig. 8. τ^*_{max} vs. α for the three considered distributions with C and D operating conditions to be simulated.

TABLE IV
CLUSTERS PARAMETERS

	Cluster Nº1		
r_s	$[0.1, 0.125, 0.025]\Omega$	I_{rate}	$[5, 2.5, 2.5]$
L	$[2.25, 2.25, 2.25]$ mH	P_{distr}	$[0.6, 1, 0.3, 0.25]$
C_b	$[0.58, 0.85, 0.17]$ mF		
	Cluster Nº2		
r_s	$[0.2, 0.3]\Omega$	I_{rate}	$[2.5, 5]$
L	$[1.8, 1.8]$ mH	P_{distr}	$[0.5, 0.5]$
C_b	$[0.4, 0.6]$ mF		
	Cluster Nº3		
r_s	$[0.06, 0.1, 0.04, 0.05]\Omega$	I_{rate}	$[4, 3, 2, 1]$
L	$[6.0, 6.0, 6.0, 6.0]$ mH	P_{distr}	$[0.25, 0.4, 0.15, 0.2]$
C_b	$[0.3, 0.5, 0.2, 0.2]$ mF		
	Cluster Nº4		
r_s	$[0.2, 0.1, 0.15, 0.05]\Omega$	I_{rate}	$[4, 3, 2, 1]$
L	$[3.2, 3.2, 3.2, 3.2]$ mH	P_{distr}	$[0.4, 0.2, 0.3, 0.1]$
C_b	$[0.4, 0.2, 0.3, 0.1]$ mF		
	All Clusters		
k_{VI}	30	a_{ij}	10
k_{CP}	10	τ_k	$10 \pm 10\%$ ms[1]
k_{CI}	1000		

[1] According to the inner cluster time delays values reported in [11], [18], [22].

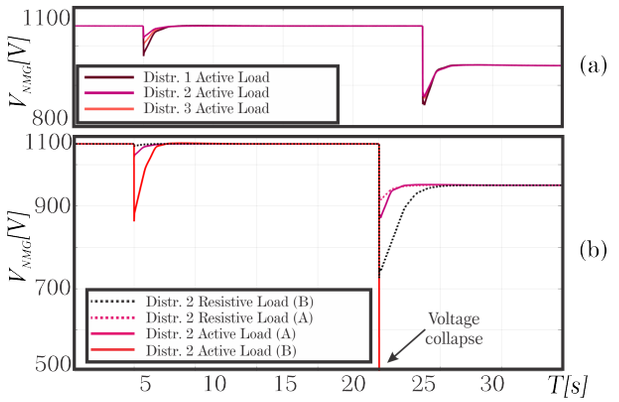

Fig. 9. (a) v_{NMG} under operating condition (A). (b) v_{NMG} under operating conditions (A) and (B). Solid lines: CPLs; dotted lines: passive loads.

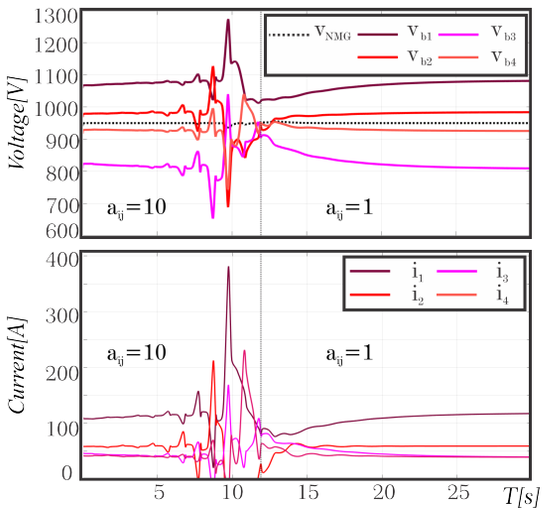

Fig. 10. v_{NMG}, v_{bk} of the individual clusters, and i_k for a small-signal load perturbation under conditions (A) and (B).

IV, they provide valuable insights into system dynamics. The fixed simulation parameters are listed in Table IV.

A. Voltage Collapse Simulation

This first set of simulations aims to evaluate the behavior of the NMG under different regions depicted in Fig. 5. Fig. 9(a) shows the time evolution of v_{NMG} under operating conditions denoted as (A) in Fig. 5, considering three different power distribution schemes from Table III. At $t = 5\,\text{s}$, the NMG transitions from a no-load condition to a minimal-load state, and at $t = 25\,\text{s}$, it shifts from a minimal-load condition to a maximal-load scenario ($P_{tot} = \overline{P_{tot}}$ and $v_{bk}^{eq} = \underline{v_{bk}}$ for $k = 1, ..., n$). As observed, a balanced distribution (Distr. Nº2) improves the system's transient response during abrupt load changes, enabling the system to handle larger loads.

The second set of simulations, presented in Fig. 9(b), aims to compare the behavior of v_{NMG} under two operating conditions, denoted as (A) and (B) in Fig. 5. The sequence of events is as described for Fig. 9(a). In comparison, the NMG with resistive loads remains stable in both scenarios, while the NMG with CPLs can only recover from the load step in scenario (A). This behavior aligns with the results shown in Fig. 5, where a stable response was expected for both systems under (A) conditions, but only for the system with resistive loads under (B) conditions. In the unstable scenario with CPLs, rather than experiencing a progressive divergence of v_{NMG}, the system collapses (see Distr. 2 (B)). This phenomenon, known as voltage collapse, occurs when the system does not have a real and constant steady state to which it can converge [7].

B. Controller Tuning

This second simulation aims to evaluate the system's response to perturbations under an operating condition of uncertain stability and subsequent stabilization by adjusting the operating points.

Fig. 10 shows the time evolution of the NMG voltages and the total current injected into local cluster buses. The NMG operates under conditions considered uncertain according to formulation (A) in Fig. 6(c), with a 5% perturbation in P_{tot} at $t = 0\,\text{s}$. The system is then brought to stable operating conditions (B) by adjusting the gains (a_{ij}) from 10 to 1 at $t = 12\,\text{s}$. Initially, under operating conditions (A),

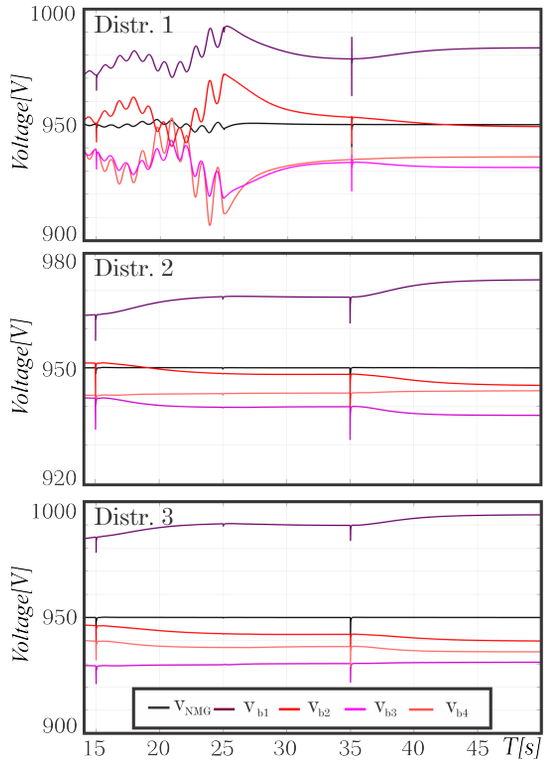

Fig. 11. v_{NMG} and v_{b_k} for a small-signal load perturbation under conditions (C) and (D) in Fig. 8, considering the three power distributions shown in Table III.

the individual bus voltages (v_{b_k}) and injected currents (i_k) diverge in an attempt to maintain the desired NMG voltage (v_{NMG}). When the system transitions to stable operating conditions (B), it progressively converges toward a stable state. This scenario aligns with the expected behavior according to Fig.6(c), where only stable behavior was predicted for (B) conditions. These observations highlight that the system exhibits uncertain behavior outside the feasible zones defined by the formulation. While previous simulations showed collapse under uncertain conditions, this scenario demonstrates non-convergence without collapse.

C. CPLs - Resistive Proportion

The simulation presented in this section was conducted to assess the system's response to perturbations under different operating conditions, distinguished solely by the balance between CPLs and resistive loads. The NMG was configured with the parameters used to obtain the curves in Fig. 8. As illustrated in Fig. 11, the simulation comprises the following steps:

- For $t < 15\,\mathrm{s}$, the system operates under the operating condition (C).
- At $t = 15\,\mathrm{s}$, a small-signal load perturbation is introduced to observe the system's behavior in the vicinity of point (C).
- At $t = 25\,\mathrm{s}$, the balance between constant power loads (CPLs) and resistive loads (α in Fig. 11) is adjusted to achieve the operating point denoted as (D) in Fig. 8.
- At $t = 40\,\mathrm{s}$, the same small-signal load perturbation as at $t = 15\,\mathrm{s}$ is applied to evaluate the system's stability at point (D).

The simulation results confirm the analytical findings shown in Fig. 8, highlighting that higher proportions of resistive loads on the total power load enhance system stability and reduces sensitivity to load variations. It is also verified that, for the conditions considered at operating point (C), only Distr. 1 exhibits unstable behavior.

VI. Conclusions

This paper presented a stability analysis for a NMG with distributed control and uncertain loads. A set of conditions was derived to evaluate system stability using a robust approach, considering the nature of loads (impedance loads, current loads, and power loads) and time delays, extending the studies conducted in previous works on this topic. The presented formulation efficiently encompasses a wide range of operating scenarios in a concise manner.

Simulations highlighted the critical roles of load characteristics, their distribution among clusters, controller tuning, and the design of consensus gains. The findings indicate that CPLs significantly impact NMG stability compared to resistive loads. Systems with CPLs require stricter operating conditions, are more sensitive to load distribution, and have reduced feasible ranges for controller and consensus gains. These elements are central to achieving stable NMG operation and resilience against different load types and communication network time delays. Simulations were also carried out to contrast the stability conditions predicted by the formulation. Also, different changes in the operating point of the system were simulated, verifying that the system became stable when it was brought to some of the conditions established as stable, even starting from initially uncertain conditions. This consistency in the results also allows validating the simplifications made to obtain the reduced order system used in the formulation. Additionally, the complexity associated with the circuit evaluation of the different cases studied highlights the usefulness of having an analytical formulation for the robust stability analysis of the microgrid. This formulation allows drawing conclusions and generating representations of the stable operating conditions using a reduced-order model.

VII. Appendix

The system dynamics described by equations (8)-(13) can be rewritten in a matrix representation as shown in equation (14) by defining the following:

$$\mathbf{A} = \begin{bmatrix} -(\mathbf{L_E}+\mathbf{G}).\mathbf{C2} & \mathbf{0} & \mathbf{C} & \mathbf{0} \\ -\frac{1}{n}\mathbf{K_{IV}} & \mathbf{0} & -\mathbf{K_{II}}.\mathbf{I_r} & \mathbf{K_{II}} - \mathbf{K_{PI}}.diag(\mathbf{L_A}) \\ -\mathbf{L} & \mathbf{L} & -\mathbf{R_{sk}}.\mathbf{L} & \mathbf{0} \\ -\mathbf{I_r}.\mathbf{L} & \mathbf{I_r}.\mathbf{L} & -\mathbf{R_{sk}}.\mathbf{L}.\mathbf{I_r} & -diag(\mathbf{L_A}) \end{bmatrix} \quad (35)$$

$$\mathbf{B} = \begin{bmatrix} \mathbf{0} & \mathbf{0} & \mathbf{0} & \mathbf{0} \\ -\frac{1}{n}\mathbf{K_{IV2}} & \mathbf{0} & \mathbf{0} & -\mathbf{K_{PI}}.(\mathbf{L_A} - diag(\mathbf{L_A})) \\ \mathbf{0} & \mathbf{0} & \mathbf{0} & \mathbf{0} \\ \mathbf{0} & \mathbf{0} & \mathbf{0} & -(\mathbf{L_A} - diag(\mathbf{L_A})) \end{bmatrix} \quad (36)$$

$$\mathbf{H_1} = \begin{bmatrix}\mathbf{0}, \mathbf{K_{IV}}, \mathbf{L}, \mathbf{0}\end{bmatrix}^T \ \mathbf{H_2} = \begin{bmatrix}-\mathbf{C}, \mathbf{0}, \mathbf{0}, \mathbf{0},\end{bmatrix}^T \quad (37)$$

where,

$$\mathbf{G} = diag([g_{load_1} + g_{cpl_1},\ g_{load_2} + g_{cpl_2},\ \ldots, [g_{load_{n-1}} + g_{cpl_{n-1}},\ g_{load_n} + g_{cpl_n}])$$

$$\mathbf{C} = diag(\begin{bmatrix}\frac{1}{C_{b1}}, & \frac{1}{C_{b2}}, & \ldots & \frac{1}{C_{bn}}\end{bmatrix}) \quad (38)$$

$$\mathbf{C2} = \mathbf{C} * ones(n, n) \quad (39)$$

$$\mathbf{L} = diag(\begin{bmatrix}\frac{1}{L_{s1}}, & \frac{1}{L_{s2}}, & \ldots & \frac{1}{L_{sn}}\end{bmatrix}) \quad (40)$$

$$\mathbf{R_{sk}} = diag(\begin{bmatrix}r_{s1}, & r_{s2}, & \ldots & r_{sn}\end{bmatrix}) \quad (41)$$

$$\mathbf{I_r} = diag(\begin{bmatrix}\frac{1}{I_{rate_1}}, & \frac{1}{I_{rate_2}}, & \ldots & \frac{1}{I_{rate_n}}\end{bmatrix}) \quad (42)$$

$$\mathbf{K_{IV}} = diag(\begin{bmatrix}k_{iv_1}, & k_{iv_2}, & \ldots & k_{iv_n}\end{bmatrix}) \quad (43)$$

$$\mathbf{K_{IV2}} = \mathbf{K_{IV}} * ones(n, n); \quad (44)$$

$$\mathbf{K_{II}} = diag(\begin{bmatrix}k_{ii_1}, & k_{ii_2}, & \ldots & k_{ii_n}\end{bmatrix}) \quad (45)$$

$$\mathbf{K_{PI}} = diag(\begin{bmatrix}k_{pi_1}, & k_{pi_2}, & \ldots & k_{pi_n}\end{bmatrix}) \quad (46)$$

The matrices $\mathbf{L_E}$ and $\mathbf{L_A}$ have the following format:

$$\mathbf{L}_\lambda = \begin{bmatrix} \sum_j \lambda_{1j} & -\lambda_{12} & \ldots & \ldots & -\lambda_{1n} \\ * & \sum_j \lambda_{2j} & -\lambda_{23} & \ldots & -\lambda_{2n} \\ \vdots & \vdots & \ddots & \ldots & \vdots \\ * & * & * & \ldots & \sum_j \lambda_{nj} \end{bmatrix} \quad (47)$$

with $\lambda = g$, for $\mathbf{L_E}$, and, $\lambda = a$, for $\mathbf{L_A}$.

$$\mathbf{0} = zeros(n, n) \quad (48)$$

REFERENCES

[1] M. Shafiullah, A. Refat, M. E. Haque, D. M. H. Chowdhury, S. Hossain, A. Alharbi, S. Alam, A. Ali, and S. Hossain, "Review of recent developments in microgrid energy management strategies," *Sustainability*, vol. 14, pp. 1–30, 11 2022, doi: 10.3390/su142214794.

[2] Q. Zhou, M. Shahidehpour, A. Paaso, S. Bahramirad, A. Alabdulwahab, and A. Abusorrah, "Distributed control and communication strategies in networked microgrids," *IEEE Communications Surveys & Tutorials*, vol. 22, no. 4, pp. 2586–2633, 2020, doi: 10.1109/COMST.2020.3023963.

[3] J. Liu, W. Zhang, and G. Rizzoni, "Robust stability analysis of dc microgrids with constant power loads," *IEEE Trans. Power Syst.*, vol. 33, no. 1, pp. 851–860, 2018, doi: 10.1109/TPWRS.2017.2697765.

[4] M. Jeeninga, C. De Persis, and A. van der Schaft, "Dc power grids with constant-power loads—part i: A full characterization of power flow feasibility, long-term voltage stability, and their correspondence," *IEEE Transactions on Automatic Control*, vol. 68, no. 1, pp. 2–17, 2023, doi: 10.1109/TAC.2022.3157076.

[5] Z. Liu, M. Su, Y. Sun, X. Zhang, X. Liang, and M. Zheng, "A comprehensive study on the existence and stability of equilibria of dc-distribution networks with constant power loads," *IEEE Transactions on Automatic Control*, vol. 67, no. 4, pp. 1988–1995, 2022, doi: 10.1109/TAC.2021.3072084.

[6] J. Liu, Y. Zhang, A. J. Conejo, and F. Qiu, "Ensuring transient stability with guaranteed region of attraction in dc microgrids," *IEEE Transactions on Power Systems*, vol. 38, no. 1, pp. 681–691, 2023, doi: 10.1109/TPWRS.2022.3167315.

[7] Z. Liu, M. Su, Y. Sun, W. Yuan, H. Han, and J. Feng, "Existence and stability of equilibrium of dc microgrid with constant power loads," *IEEE Trans. Power Syst.*, vol. 33, no. 6, pp. 6999–7010, 2018, doi: 10.1109/TPWRS.2018.2849974.

[8] M. Carnaghi, P. Cervellini, M. Judewicz, R. Garcia Retegui, and M. Funes, "Stability analysis of a networking dc microgrid with distributed droop control and cpls," *IEEE Latin America Transactions*, vol. 21, no. 9, p. 966–975, Sep. 2023. [Online]. Available: https://latamt.ieeer9.org/index.php/transactions/article/view/7810

[9] M. Dong, L. Li, Y. Nie, D. Song, and J. Yang, "Stability analysis of a novel distributed secondary control considering communication delay in dc microgrids," *IEEE Transactions on Smart Grid*, vol. 10, no. 6, pp. 6690–6700, 2019, doi: 10.1109/TSG.2019.2910190.

[10] A. B. Shyam, S. Anand, and S. R. Sahoo, "Effect of communication delay on consensus-based secondary controllers in dc microgrid," *IEEE Trans. Ind. Electron.*, vol. 68, no. 4, pp. 3202–3212, 2021, doi: 10.1109/TIE.2020.2978719.

[11] W. Yao, Y. Wang, Y. Xu, and C. Dong, "Small-signal stability analysis and lead-lag compensation control for dc networked-microgrid under multiple time delays," *IEEE Trans. Power Syst.*, vol. 38, no. 1, pp. 921–933, 2023, doi: 10.1109/TPWRS.2022.3169821.

[12] Z. Liu, M. Su, Y. Sun, H. Han, X. Hou, and J. M. Guerrero, "Stability analysis of dc microgrids with constant power load under distributed control methods," *Automatica*, vol. 90, p. 62–72, Apr. 2018, doi: 10.1016/j.automatica.2017.12.051. [Online]. Available: http://dx.doi.org/10.1016/j.automatica.2017.12.051

[13] M. Carnaghi, P. Cervellini, R. G. Retegui, M. Judewicz, and M. Funes, "Analysis of constant power loads impact on dc microgrid with distributed control," in *2022 IEEE Biennial Congress of Argentina (ARGENCON)*, 2022, doi: 10.1109/ARGENCON55245.2022.9939879, pp. 1–7.

[14] D. Liu, K. Jiang, L. Yan, X. Ji, K. Cao, and P. Xiong, "A fully distributed economic dispatch method in dc microgrid based on consensus algorithm," *IEEE Access*, vol. 10, pp. 119 345–119 356, 2022, doi: 10.1109/ACCESS.2022.3221435.

[15] W. Xie, M. Han, W. Cao, J. M. Guerrero, and J. C. Vasquez, "System-level large-signal stability analysis of droop-controlled dc microgrids," *IEEE Trans. Power Electron.*, vol. 36, no. 4, pp. 4224–4236, 2021, doi: 10.1109/TPEL.2020.3019311.

[16] S. Liu, X. Li, M. Xia, Q. Qin, and X. Liu, "Takagi-sugeno multimodeling-based large signal stability analysis of dc microgrid clusters," *IEEE Trans. Power Electron.*, vol. 36, no. 11, pp. 12 670–12 684, 2021, doi: 10.1109/TPEL.2021.3076734.

[17] R. Han, M. Tucci, A. Martinelli, J. M. Guerrero, and G. Ferrari-Trecate, "Stability analysis of primary plug-and-play and secondary leader-based controllers for dc microgrid clusters," *IEEE Trans. Power Syst.*, vol. 34, no. 3, pp. 1780–1800, 2019, doi: 10.1109/TPWRS.2018.2884876.

[18] Y. Yu, G.-P. Liu, and W. Hu, "Coordinated distributed predictive control for voltage regulation of dc microgrids with communication delays and data loss," *IEEE Transactions on Smart Grid*, vol. 14, no. 3, pp. 1708–1722, 2023, doi: 10.1109/TSG.2022.3208946.

[19] Y. He, Q.-G. Wang, L. Xie, and C. Lin, "Further improvement of free-weighting matrices technique for systems with time-varying delay," *IEEE Trans. Autom. Control*, vol. 52, no. 2, pp. 293–299, 2007, doi: 10.1109/TAC.2006.887907.

[20] C. Li, F. de Bosio, S. K. Chaudhary, M. Graells, J. C. Vasquez, and J. M. Guerrero, "Operation cost minimization of droop-controlled dc microgrids based on real-time pricing and optimal power flow," in *IECON 2015 - 41st Annual Conference of the IEEE Industrial Electronics Society*, 2015, doi: 10.1109/IECON.2015.7392709, pp. 003 905–003 909.

[21] M. Grant and S. Boyd, in *Graph implementations for nonsmooth convex programs*. Springer-Verlag Limited, 2008, pp. 95–110. [Online]. Available: https://doi.org/10.1007/978-1-84800-155-8_7

[22] M. Zaery and M. A. Abido, "Distributed optimal power dispatch for islanded dc microgrids with time delays," *IEEE Access*, vol. 12, pp. 12 533–12 544, 2024, doi: 10.1109/ACCESS.2024.3356077.

Marco Carnaghi was born in Mar del Plata, Buenos Aires, Argentina, in 1996. In 2019 he received the degree of Electronic Engineer, awarded by the School of Engineering (UNMDP). He is currently a doctoral fellow at CONICET.

Marcos Judewicz was born in Mar del Plata, Buenos Aires, Argentina, en 1986. In 2011 he received the degree of Electronic Engineer from the School of Engineering (UNMDP). In 2016 he received the degree of Doctor in Engineering, electronics orientation. He is currently a researcher at CONICET.

Paula Cervellini was born in Santa Rosa, La Pampa, Argentina, in 1985. In 2014 she received the degree of Electronic Engineer, awarded by the School of Engineering (UNMDP). In 2019 she received the degree of Doctor in Engineering, electronics orientation. She is currently a researcher at CONICET.

Rogelio García Retegui was born in Tandil, Buenos Aires, Argentina, in 1977. In 2002 he received the degree of Electronic Engineer from the School of Engineering (UNMDP). In 2009 he received the degree of Doctor in Engineering, electronics orientation. He is currently a researcher at CONICET.

Marcos Funes was born in Mar del Plata, Buenos Aires, Argentina, in 1974. In 1999 he received the degree of Electronic Engineer from the School of Engineering (UNMDP). In 2007 he received the degree of Doctor in Engineering, electronics orientation. He is currently a researcher at CONICET.